www.elsevier.com/locate/ijadhadh

A general solution for the two-dimensional stress analysis of balanced and unbalanced adhesively bonded joints

Zunxu Liu, YongAn Huang, Zhouping Yin, Stefano Bennati, Paolo S. Valvo

PII: S0143-7496(14)00124-9
DOI: http://dx.doi.org/10.1016/j.ijadhadh.2014.05.011
Reference: JAAD1545

To appear in: *International Journal of Adhesion & Adhesives*

Accepted date: 19 May 2014

Cite this article as: Zunxu Liu, YongAn Huang, Zhouping Yin, Stefano Bennati, Paolo S. Valvo, A general solution for the two-dimensional stress analysis of balanced and unbalanced adhesively bonded joints, *International Journal of Adhesion & Adhesives,* http://dx.doi.org/10.1016/j.ijadhadh.2014.05.011

A general solution for the two-dimensional stress analysis of balanced and unbalanced adhesively bonded joints

Zunxu LIU[a], YongAn HUANG[a,*], Zhouping YIN[a,*] Stefano BENNATI[b], Paolo S. VALVO[b]

[a] *State Key Laboratory of Digital Manufacturing Equipment and Technology, Huazhong University of Science and Technology, Wuhan, 430074, China*

[b] *Department of Civil and Industrial Engineering, University of Pisa, Largo Lucio Lazzarino, I-56126 Pisa, Italy*

Abstract

This paper presents an efficient analytical solution strategy to determine the adhesive stresses in balanced and unbalanced adhesively bonded joints with mixed force loading and/or displacement boundary conditions. The adhesive stresses are expressed in terms of geometrical dimensions and material properties, combined with integration constants obtained numerically. The model is successfully applied for the analysis of various types of joints, including balanced and unbalanced stiffened plate/joint, single-strap joint, and single-lap joint. In all such cases, the linear equation sets are supplied to determine the integration constants in the final stress expressions. The analytical predictions agree well with the finite element results for adhesive stresses. This proposed model can be extended conveniently to predict the mechanical behaviour of similar bonded structures such as composite laminates, electronics packaging, and flexible electronics structures.

Keywords: Stress analysis; analytical solution; adhesively bonded joints; stiffened plate/joint; single-strap joint; single-lap joint.

1. Introduction

Adhesively bonded joints have found extensive applications for load transfer and connection elements in aerospace, mechanical, and civil engineering structures [1], for structural repairing [2] and for surface-bonded piezoelectric smart structures [3]. Recently, they play increasingly important roles in flexible electronics design [4] and microelectronics packaging [5, 6]. Adhesive joints generally consist of three layers: two adherends and an adhesive layer. Due to the discontinuity of the layers at the edges, complicated stress fields and high stress concentrations usually occur in the vicinity of the corners of the adhesive layers. Such high adhesive stresses often result in local yielding of the adhesive and crack propagation in the adhesive or at the adhesive/adherend

* Corresponding authors.
Tel: +8613545354545; fax: +86 27 87543072.
E-mail address: yahuang@hust.edu.cn (YongAn Huang); yinzhp@mail.hust.edu.cn (Zhouping Yin).

interfaces, and may finally lead to the overall failure of the joint. Therefore, efficient and reasonably accurate estimation of the stress level in adhesively bonded joints is crucial for joint design and structural safety evaluation as well as for a better understanding of the underlying mechanisms of failure.

Over the decades, there has been a wide body of literature on the analysis of adhesively bonded joints typically including, in particular, stiffened plate/joint [5-8], single-strap joint [8-10] , and single-lap joint [11-20]. Detailed reviews on the historical development of both analytical models and finite element method (FEM) for stress analysis of joints can be found in the recent review papers by da Silva et al. [21, 22] and He [23]. The overwhelming majority of the aforementioned works focus on the singe-lap joint configuration. The pioneering works by Goland and Reissner [11] furnished the classical solution for the adhesive stresses in joints subjected to mechanical loads. Further improvements have been presented by Hart-Smith [12], Adams and Mallick. [16], and Tsai et al. [17, 18], etc. In an attempt to rationalize the analysis of bonded joints under pure force loading, Bigwood and Crocombe further derived a general elastic analysis [24]. In addition, a large number of experimental studies involving the strength predictions of the single-lap joints were made as well [25-29]. The stiffened and single-strap joint configurations, however, have received little attention. Relevant work on the deformation analysis of the singe-strap joint has been carried out by Shahin et al. [9] and Li [10], etc. By comparing the reported models, it is found that with releasing the assumptions, the governing equations become increasingly complicated, so that it is challengeable to obtain closed-form expressions for the solution to the differential problem. In such cases, one strategy is to obtain approximate closed-form solutions for relatively simple and/or extremely simplified structures. Another strategy is to solve numerically the differential equations. A similar modelling approach can be adopted to study the analogous problem of the delamination of composite laminates [30]. Accordingly, a delaminated laminate is modelled as an assemblage of sublaminates, connected by a deformable (in most cases, a linearly elastic) interlaminar interface. In such cases, the interface is not necessarily representative of a physical adhesive layer, but is introduced into the model to take into account conventionally the transverse deformability of the laminates, which is neglected in models based on Euler-Bernoulli's simple beam theory. The authors have used this modelling approach to develop an enhanced beam-theory (EBT) model of the asymmetric double cantilever beam (ADCB) test, for which a numerical-analytical solution strategy has been proposed [31]. Recently, an EBT model has been developed also for the mixed-mode bending (MMB) test [32, 33]. Furthermore, the model has been extended to general layered structures, showing how the same analytical solution can be used to describe both delaminated laminates and joints [34].

Actually, even though adhesively bonded joints have been intensively investigated over the past decades,

more attentions were paid to modelling the overlap region with pure force loading at the adherend ends, namely, consisting of tensile and shear forces and bending moment components. In this paper, we present a general mechanical model and a related solution strategy, which are expected to provide an efficient methodology to model different bonded joints under mixed (force and/or displacement) boundary conditions. It is possible not only to obtain the analytical expressions for the adhesive stresses but also internal forces, displacements, strain and stress components in the adherends. The layout of the paper is as follows. Section II describes the mechanical model and provides the theoretical framework of our solution strategy for general adhesively bonded joints. Then the coupled differential problem is solved by conveniently assuming the adhesive stresses as the main unknowns, to obtain a complete analytical solution for the adhesive stresses, internal forces and displacements. Section III describes how to apply the force and/or displacement boundary conditions to obtain the integration constants for various balanced and unbalanced adhesively bonded joints, including the stiffened plate/joint, single-strap joint, and single-lap joint. Lastly, in Section IV the effectiveness and accuracy of the proposed solution strategy are verified by comparison of the predicted adhesive stresses with those computed by using the FEM and other analytical solutions of the literature. Finally, Section V draws the conclusions

2. Formulation of the problem

2.1. Adhesive model in the overlap joints

Generally speaking, overlap joints consist of two slender adherend layers, whose materials may be identical or different from each other, bonded through a thin adhesive layer as sketched in Fig. 1(a). The thicknesses of the upper and lower adherends are denoted by H_1 and H_2, respectively, and the thickness of the adhesive layer in between is h_a, with $h_a << H_1, H_2$. Considering a linear elastic body, the materials are assumed isotropic, and the corresponding elastic modulus and Poisson's ratio are E_1, ν_1, and E_2, ν_2 for the adherends, and E_a, ν_a for the adhesive. Local coordinate systems are fixed with their origins at the mid-planes of both adherends. The x-coordinate measures the distance in the axial direction, while local axes z_1 and z_2 denote the distances in the transverse direction from the mid-planes of adherends 1 and 2, respectively. Accordingly, we indicate with u_i and w_i the mid-plane displacements of the substrates along the axial and transverse directions, respectively, and with ϕ_i the rotations of their cross sections, positive if counter-clockwise (here, and in the following, i = 1, 2 refer to the upper and lower adherends, respectively). In what follows, we consider a unit width in the y-direction (namely, normal to the plane of the figure) and assume plane strain conditions for all the elastic elements involved.

According to Timoshenko's beam theory the axial and transverse displacements at a point inside the

adherends are given by $U_i(x,z_i)=u_i(x)+z_i\phi_i(x)$ and $W_i(x,z_i)=w_i(x)$. As mentioned, we neglect any variation of the stresses and strains in the adhesive layer along the *z*-direction. In particular, the strain components at a point in the adhesive are approximated by their mean values computed from the relative displacements at the top and bottom surfaces of the adherends. Hence:

$$\begin{cases}\varepsilon_{zz}^{a}=\dfrac{W_2^{\text{top}}-W_1^{\text{bottom}}}{h_a}=\dfrac{W_2\big|_{z_2=-h_2}-W_1\big|_{z_1=h_1}}{h_a}=\dfrac{w_2-w_1}{h_a},\\ \gamma_{xz}^{a}=\dfrac{U_2^{\text{top}}-U_1^{\text{bottom}}}{h_a}=\dfrac{U_2\big|_{z_2=-h_2}-U_1\big|_{z_1=h_1}}{h_a}=\dfrac{u_2-u_1-h_1\phi_1-h_2\phi_2}{h_a},\end{cases} \tag{1}$$

where $h_1 = H_1/2$ and $h_2 = H_2/2$ are the half thicknesses of the adherends. Under plane strain conditions, if we assume that the adhesive longitudinal normal stress is negligible, only transverse normal (peel) and shear stresses exist in the adhesive. Hooke's law yields the adhesive peel and shear stresses as $\sigma = E_a^{*}\varepsilon_{zz}^{a}$ and $\tau = G_a\gamma_{xz}^{a}$, respectively, where $E_a^{*} = E_a/(1-\nu_a^2)$ and $G_a = E_a/[2(1+\nu_a)]$ are the elastic modulus (in plane strain) and shear modulus of the adhesive. Based on the aforementioned assumptions, the adhesive layer consists of a uniform, continuous distribution of springs acting in the normal and tangential directions with respect to the interface plane. Accordingly, we define the peel stiffness, k_σ, and shear stiffness, k_τ. A simple, yet effective estimate of the latter constants is given by $k_\sigma = E_a^{*}/h_a$ and $k_\tau = G_a/h_a$, Therefore:

$$\begin{cases}\sigma=k_\sigma\left(w_2-w_1\right),\\ \tau=k_\tau\left(u_2-u_1-h_1\phi_1-h_2\phi_2\right).\end{cases} \tag{2}$$

2.2. Equilibrium equations

Fig. 1(b) shows free-body diagrams of infinitesimal adherends and adhesive elements, describing the forces and moments as well as the peel and shear adhesive stresses. Considering the three equilibrium requirements for each adherend, the following differential equations hold:

$$\begin{cases}\dfrac{\mathrm{d}N_1}{\mathrm{d}x}+\tau=0, \quad \dfrac{\mathrm{d}Q_1}{\mathrm{d}x}+\sigma=0, \quad \dfrac{\mathrm{d}M_1}{\mathrm{d}x}+h_1\tau-Q_1=0;\\ \dfrac{\mathrm{d}N_2}{\mathrm{d}x}-\tau=0, \quad \dfrac{\mathrm{d}Q_2}{\mathrm{d}x}-\sigma=0, \quad \dfrac{\mathrm{d}M_2}{\mathrm{d}x}+h_2\tau-Q_2=0;\end{cases} \tag{3}$$

where N_i, Q_i, and M_i denote the axial force, shear force, and bending moment per unit width, respectively. The internal forces are given by the constitutive laws of a Timoshenko's beam:

$$N_i=A_i\frac{\mathrm{d}u_i}{\mathrm{d}x}, \quad Q_i=C_i\left(\frac{\mathrm{d}w_i}{\mathrm{d}x}+\phi_i\right), \quad M_i=D_i\frac{\mathrm{d}\phi_i}{\mathrm{d}x}, \tag{4}$$

where $A_i = A_{11}^{i}$, $C_i = k_s A_{55}^{i}$, and $D_i = D_{11}^{i}$ respectively are the adherends' extensional stiffness, shear stiffness, and bending stiffness. In particular, $A_i = E_i^{*}H_i$, $C_i = k_s G_i H_i$, and $D_i = E_i^{*}H_i^3/12$ for isotropic adherends, in which $E_i^{*} = E_i/(1-\nu_i^2)$ and $G_i = E_i/[2(1+\nu_i)]$ are the effective Young's modulus (in plane strain) and shear modulus,

respectively. k_s is the shear correction factor. In addition, we define the corresponding compliances, $a_i = 1/A_i$, $c_i = 1/C_i$, and $d_i = 1/D_i$. By substituting Eq. (4) into (3), we derive the following governing differential equations, which establish a relationship between the adherends' displacements and the adhesive stresses:

$$\begin{cases} \dfrac{\mathrm{d}^2 u_1}{\mathrm{d}x^2} = -a_1\tau; \quad \dfrac{\mathrm{d}\phi_1}{\mathrm{d}x} + \dfrac{\mathrm{d}^2 w_1}{\mathrm{d}x^2} = -c_1\sigma; \quad \dfrac{\mathrm{d}^3\phi_1}{\mathrm{d}x^3} = -d_1\sigma - d_1 h_1 \dfrac{\mathrm{d}\tau}{\mathrm{d}x}; \\ \dfrac{\mathrm{d}^2 u_2}{\mathrm{d}x^2} = a_2\tau; \quad \dfrac{\mathrm{d}\phi_2}{\mathrm{d}x} + \dfrac{\mathrm{d}^2 w_2}{\mathrm{d}x^2} = c_2\sigma; \quad \dfrac{\mathrm{d}^3\phi_2}{\mathrm{d}x^3} = d_2\sigma - d_2 h_2 \dfrac{\mathrm{d}\tau}{\mathrm{d}x}. \end{cases} \tag{5}$$

2.3. Adhesive stresses

Generally, the adhesive stresses are conveniently considered as main unknowns. The two equations in the Eq. (2) are respectively differentiated with respect to x four and three times, subsequently Eqs. (5) are introduced and the following differential equation set is obtained:

$$\begin{cases} \dfrac{\mathrm{d}^4\sigma}{\mathrm{d}x^4} - k_\sigma\left(c_1 + c_2\right)\dfrac{\mathrm{d}^2\sigma}{\mathrm{d}x^2} + k_\sigma\left(d_1 + d_2\right)\sigma + k_\sigma\left(d_1 h_1 - d_2 h_2\right)\dfrac{\mathrm{d}\tau}{\mathrm{d}x} = 0, \\ \dfrac{\mathrm{d}^3\tau}{\mathrm{d}x^3} - k_\tau\left(a_2 + a_1 + d_2 h_2^2 + d_1 h_1^2\right)\dfrac{\mathrm{d}\tau}{\mathrm{d}x} - k_\tau\left(d_1 h_1 - d_2 h_2\right)\sigma = 0. \end{cases} \tag{6}$$

Two cases have to be considered in solving the differential problem:

a) $d_1 h_1 = d_2 h_2$, or $E_1^* H_1^2 = E_2^* H_2^2$, which is the 'Balanced' case, certainly including the case of identical adherends;

b) $d_1 h_1 \neq d_2 h_2$, or $E_1^* H_1^2 \neq E_2^* H_2^2$, which is the 'Unbalanced' or general case.

The subscripts and superscripts 'B' and 'U' will be used in the following to denote quantities corresponding to the 'Balanced' and 'Unbalanced' cases, respectively.

2.3.1. Balanced case

In the balanced case, Eqs. (6) are uncoupled and can be written as:

$$\begin{cases} \dfrac{\mathrm{d}^4\sigma}{\mathrm{d}x^4} + \eta_1^{\mathrm{B}}\dfrac{\mathrm{d}^2\sigma}{\mathrm{d}x^2} + \eta_2^{\mathrm{B}}\sigma = 0, \\ \dfrac{\mathrm{d}^3\tau}{\mathrm{d}x^3} + \eta_3^{\mathrm{B}}\dfrac{\mathrm{d}\tau}{\mathrm{d}x} = 0, \end{cases} \tag{7}$$

where, $\eta_1^{\mathrm{B}} = -k_\sigma\left(c_1 + c_2\right)$, $\eta_2^{\mathrm{B}} = k_\sigma\left(d_1 + d_2\right)$ and $\eta_3^{\mathrm{B}} = -k_\tau\left(a_2 + a_1 + d_2 h_2^2 + d_1 h_1^2\right)$. Eqs. (7)can be solved separately to obtain the adhesive peel and shear stresses as:

$$\begin{cases} \sigma_{\mathrm{B}}(x) = \displaystyle\sum_{n=1}^{4} F_n^{\mathrm{B}} \exp\left(\lambda_n^{\mathrm{B}} x\right), \\ \tau_{\mathrm{B}}(x) = \displaystyle\sum_{n=5}^{6} F_n^{\mathrm{B}} \exp\left(\lambda_n^{\mathrm{B}} x\right) + F_7^{\mathrm{B}}, \end{cases} \tag{8}$$

where F_1^{B}, F_2^{B}, …, F_7^{B} are integration constants to be determined by imposing the boundary conditions; λ_1^{B},

λ_2^{B}, λ_3^{B} and λ_4^{B} are the roots of the characteristic equation, $\lambda^4+\eta_1^{\mathrm{B}}\lambda^2+\eta_2^{\mathrm{B}}=0$; and $\lambda_5^{\mathrm{B}}=\sqrt{-\eta_3^{\mathrm{B}}}$ and $\lambda_6^{\mathrm{B}}=-\sqrt{-\eta_3^{\mathrm{B}}}$ are other two real characteristic roots.

2.3.2. Unbalanced case

In the unbalanced case, uncoupling of Eqs. (6) is obtained by solving the first equation for dτ/dx and substituting the result into the second equation. A sixth-order linear homogeneous differential equation for the peel stress is obtained:

$$\frac{\mathrm{d}^6\sigma}{\mathrm{d}x_1^6}+\eta_1^{\mathrm{U}}\frac{\mathrm{d}^4\sigma}{\mathrm{d}x_1^4}+\eta_2^{\mathrm{U}}\frac{\mathrm{d}^2\sigma}{\mathrm{d}x_1^2}+\eta_3^{\mathrm{U}}\sigma=0, \tag{9}$$

where $\eta_1^{\mathrm{U}}=-k_\tau\left(a_1+a_2+d_1h_1^2+d_2h_2^2\right)-k_\sigma\left(c_1+c_2\right)$, $\eta_2^{\mathrm{U}}=k_\tau k_\sigma\left(a_1+a_2+d_1h_1^2+d_2h_2^2\right)\left(c_1+c_2\right)+k_\sigma\left(d_1+d_2\right)$, and $\eta_3^{\mathrm{U}}=-k_\tau k_\sigma\left[\left(a_1+a_2\right)\left(d_1+d_2\right)+d_1d_2\left(h_1+h_2\right)^2\right]$. By solving Eq. (9), and substituting the result into the first term of Eq. (6), the general expressions for the adhesive peel and shear stresses are obtained:

$$\begin{cases}\sigma_{\mathrm{U}}\left(x\right)=\displaystyle\sum_{n=1}^{6}F_n^{\mathrm{U}}\exp\left(\lambda_n^{\mathrm{U}}x\right),\\ \tau_{\mathrm{U}}\left(x\right)=-\dfrac{1}{d_1h_1-d_2h_2}\left\{\displaystyle\sum_{n=1}^{6}F_n^{\mathrm{U}}\left[\frac{\left(\lambda_n^{\mathrm{U}}\right)^3}{k_\sigma}-\left(c_1+c_2\right)\lambda_n^{\mathrm{U}}+\frac{d_1+d_2}{\lambda_n^{\mathrm{U}}}\right]\exp\left(\lambda_n^{\mathrm{U}}x\right)+F_7^{\mathrm{U}}\right\},\end{cases} \tag{10}$$

where F_1^{U}, F_2^{U}, …, F_7^{U} are integration constants; λ_1^{U}, λ_2^{U}, ..., λ_6^{U} are the roots of the characteristic equation, $\lambda^6+\eta_1^{\mathrm{U}}\lambda^4+\eta_2^{\mathrm{U}}\lambda^4+\eta_3^{\mathrm{U}}=0$.

2.4. Internal forces and displacements

The internal force expressions, in the balanced case, can be deduced by substituting Eqs. (8) into Eqs. (3), and integrating with respect to x. In turn, by substituting the internal forces into Eqs. (4) and integrating with respect to x, the expressions of the displacement are also derived. In this process, twelve new integration constants, F_8^{B}, F_9^{B}, …, F_{19}^{B}, appear. On the other hand, for the more general case, the analytical expressions for the internal forces and displacements, involving twelve more constants, F_8^{U}, F_9^{U}, ..., F_{19}^{U}, can also be obtained in the same way. The details can be found in Appendix A.1.

3. Integration constants for various adhesively bonded joints

To sum up, the complete solution to the differential problem depends upon 19 integration constants for both the balanced and unbalanced cases. However, such constants are not all independent of each other. Actually, by introducing the expressions for the adhesive stresses and displacements into Eqs. (2), seven relationships are found among the constants (see Appendix A.2). As a consequence, 12 independent constants remain. By

imposing the suitable boundary conditions, these integration constants can be obtained by solving a linear equation set. It should be pointed out that not all of the constants can be determined in general, because of the possible existence of rigid-body displacements for the whole structure. In any case, the main interest is on the first seven constants, which enter the expressions for σ and τ, Eqs. (8) and (10).

In this section, we present the boundary conditions and the ensuing first seven integration constants for three common types of adhesively bonded joints. The expressions for the remaining integration constants are given in Appendix A.3.

3.1. Stiffened plate/joint under axial tension and/or bending moment

A typical stiffened plate/joint under axial tension and bending moment is depicted in Fig. 2(a) [6]. Due to the symmetry of the structure and loading, the analysis can be limited to the right-hand half portion shown in Fig. 2(b). The boundary conditions are stated as follows:

a) symmetry conditions at the left-hand end sections:

$$\begin{aligned} &u_1\big|_{x=0}=0, \quad \phi_1\big|_{x=0}=0, \quad Q_1\big|_{x=0}=0; \\ &u_2\big|_{x=0}=0, \quad \phi_2\big|_{x=0}=0, \quad Q_2\big|_{x=0}=0; \end{aligned} \tag{11}$$

b) free end and applied load conditions at the right-hand end sections of the upper and lower layers, respectively:

$$\begin{aligned} &N_1\big|_{x=l}=0, \quad Q_1\big|_{x=l}=0, \quad M_1\big|_{x=l}=0; \\ &N_2\big|_{x=l}=P_0, \quad Q_2\big|_{x=l}=0, \quad M_2\big|_{x=l}=-M_0. \end{aligned} \tag{12}$$

By substituting the expressions for the internal forces and displacements into Eqs. (12) and (13), and combining with the seven relationships among the constants listed in Appendix A.2, the integration constants can be obtained. For a balanced stiffened plate/joint, the first four constants included in the peel stress expression are given by the solution of the following linear equation set:

$$\begin{aligned} &\sum_{n=1}^{4} F_n^{\mathrm{B}} \frac{1}{\lambda_n^{\mathrm{B}}}=0, \\ &\sum_{n=1}^{4} F_n^{\mathrm{B}} \frac{1}{\left(\lambda_n^{\mathrm{B}}\right)^3}=0, \\ &\sum_{n=1}^{4} F_n^{\mathrm{B}} \frac{\exp\left(\lambda_n^{\mathrm{B}} l\right)}{\lambda_n^{\mathrm{B}}}=0, \\ &\sum_{n=1}^{4} F_n^{\mathrm{B}} \frac{\exp\left(\lambda_n^{\mathrm{B}} l\right)}{\left(\lambda_n^{\mathrm{B}}\right)^2}=h_1 F_8^{\mathrm{B}}-F_{10}^{\mathrm{B}}; \end{aligned} \tag{13}$$

and the two constants included in the shear stress expression are:

$$F_5^{\mathrm{B}}=-F_6^{\mathrm{B}}=-\frac{\lambda_5^{\mathrm{B}}}{2\cosh\left(\lambda_5^{\mathrm{B}} l\right)} F_8 . \tag{14}$$

Likewise, for an unbalanced stiffened plate/joint, the first six constants are obtained by the solution of the following linear equation set:

$$\begin{aligned}
&\sum_{n=1}^{6} F_n^{\mathrm{U}} \lambda_n^{\mathrm{U}} = 0, \\
&\sum_{n=1}^{6} F_n^{\mathrm{U}} \frac{1}{\lambda_n^{\mathrm{U}}} = 0, \\
&\sum_{n=1}^{6} F_n^{\mathrm{U}} \frac{1}{\left(\lambda_n^{\mathrm{U}}\right)^3} = 0, \\
&\sum_{n=1}^{6} F_n^{\mathrm{U}} \frac{\exp\left(\lambda_n^{\mathrm{U}} l\right)}{\lambda_n^{\mathrm{U}}} = 0, \\
&\sum_{n=1}^{6} F_n^{\mathrm{U}} \frac{\exp\left(\lambda_n^{\mathrm{U}} l\right)}{\left(\lambda_n^{\mathrm{U}}\right)^2} = -\frac{F_8^{\mathrm{U}} + d_2 M_0}{d_1 + d_2}, \\
&\sum_{n=1}^{6} F_n^{\mathrm{U}} \left[\frac{\left(\lambda_n^{\mathrm{U}}\right)^2}{k_\sigma} - \left(c_1 + c_2\right) \right] \exp\left(\lambda_n^{\mathrm{U}} l\right) = d_2 M_0 .
\end{aligned} \tag{15}$$

3.2. Single-strap joint under tension

Fig. 3(a) illustrates a single-strap joint under tensile loading [8]. Because of the symmetry, only one-half of the structure is modelled. The boundary conditions are stated as follows:

a) applied load and free end conditions at the left-hand end sections of the upper and lower layers, respectively:

$$\begin{aligned}
&N_1\big|_{x=0} = P_0, \quad Q_1\big|_{x=0} = 0, \quad M_1\big|_{x=0} = M_0; \\
&N_2\big|_{x=0} = 0, \quad Q_2\big|_{x=0} = 0, \quad M_2\big|_{x=0} = 0;
\end{aligned} \tag{16}$$

where $M_0 = \left(h_1 + h_2\right) P_0$ for equilibrium;

b) free end and applied load conditions at the right-hand end sections of the upper and lower layers, respectively:

$$\begin{aligned}
&N_1\big|_{x=l} = 0, \quad Q_1\big|_{x=l} = 0, \quad M_1\big|_{x=l} = 0; \\
&N_2\big|_{x=l} = P_0, \quad Q_2\big|_{x=l} = 0, \quad M_2\big|_{x=l} = 0.
\end{aligned} \tag{17}$$

Similar to Section 3.1, by imposing the boundary conditions, for a balanced single-strap joint the first four constants included in the peel stress expression are obtained as the solution of the following linear equation:

$$\begin{aligned}
&\sum_{n=1}^{4} F_n^{\mathrm{B}} \frac{1}{\lambda_n^{\mathrm{B}}} = 0, \\
&\sum_{n=1}^{4} F_n^{\mathrm{B}} \frac{1}{\left(\lambda_n^{\mathrm{B}}\right)^2} = -h_2 P_0, \\
&\sum_{n=1}^{4} F_n^{\mathrm{B}} \frac{\exp\left(\lambda_n^{\mathrm{B}} l\right)}{\lambda_n^{\mathrm{B}}} = 0, \\
&\sum_{n=1}^{4} F_n^{\mathrm{B}} \frac{\exp\left(\lambda_n^{\mathrm{B}} l\right)}{\left(\lambda_n^{\mathrm{B}}\right)^2} = 0;
\end{aligned} \tag{18}$$

while the constants appearing in the shear stress expression are

$$F_5^{\mathrm{B}}=\frac{\lambda_5^{\mathrm{B}}\left(e^{-\lambda_5^{\mathrm{B}}l}F_{11}^{\mathrm{B}}-F_8^{\mathrm{B}}\right)}{2\cosh\left(\lambda_5^{\mathrm{B}}l\right)},\quad F_6^{\mathrm{B}}=\frac{\lambda_5^{\mathrm{B}}\left(e^{\lambda_5^{\mathrm{B}}l}F_{11}^{\mathrm{B}}-F_8^{\mathrm{B}}\right)}{2\cosh\left(\lambda_5^{\mathrm{B}}l\right)}. \tag{19}$$

For an unbalanced single-strap joint, the first six constants are obtained as the solution of the following linear equation set:

$$\begin{aligned}
&\sum_{n=1}^{6}F_n^{\mathrm{U}}\frac{1}{\lambda_n^{\mathrm{U}}}=0,\\
&\sum_{n=1}^{6}F_n^{\mathrm{U}}\frac{1}{\left(\lambda_n^{\mathrm{U}}\right)^2}=-\frac{F_{11}^{\mathrm{U}}+d_1M_0}{d_1+d_2},\\
&\sum_{n=1}^{6}F_n^{\mathrm{U}}\left[\frac{\left(\lambda_n^{\mathrm{U}}\right)^2}{k_\sigma}-\left(c_1+c_2\right)\right]=d_1M_0,\\
&\sum_{n=1}^{6}F_n^{\mathrm{U}}\frac{\exp\left(\lambda_n^{\mathrm{U}}l\right)}{\lambda_n^{\mathrm{U}}}=0,\\
&\sum_{n=1}^{6}F_n^{\mathrm{U}}\frac{\exp\left(\lambda_n^{\mathrm{U}}l\right)}{\left(\lambda_n^{\mathrm{U}}\right)^2}=-\frac{F_8^{\mathrm{U}}}{d_1+d_2},\\
&\sum_{n=1}^{6}F_n^{\mathrm{U}}\left[\frac{\left(\lambda_n^{\mathrm{U}}\right)^2}{k_\sigma}-\left(c_1+c_2\right)\right]\exp\left(\lambda_n^{\mathrm{U}}l\right)=0.
\end{aligned} \tag{20}$$

3.3. Single-lap joint under tension

Lastly, the single-lap joint shown in Fig. 4(a) is analysed [11, 12]. The more general boundary conditions are written as follows:

a) applied load and free end conditions at the left-hand end sections of the upper and lower layers, respectively:

$$\begin{aligned}
&N_1\big|_{x=0}=P_0,\quad Q_1\big|_{x=0}=Q_0,\quad M_1\big|_{x=0}=M_1;\\
&N_2\big|_{x=0}=0,\quad Q_2\big|_{x=0}=0,\quad M_2\big|_{x=0}=0;
\end{aligned} \tag{21}$$

b) free end and applied load conditions at the right-hand end sections of the upper and lower layers, respectively:

$$\begin{aligned}
&N_1\big|_{x=2l}=0,\quad Q_1\big|_{x=2l}=0,\quad M_1\big|_{x=2l}=0;\\
&N_2\big|_{x=2l}=P_0,\quad Q_2\big|_{x=2l}=Q_0,\quad M_2\big|_{x=2l}=-M_2;
\end{aligned} \tag{22}$$

where $M_1=k_1(h_1+h_2)P_0$, $M_2=k_2(h_1+h_2)P_0$ and $Q_0=(1-k_1-k_2)(h_1+h_2)P_0/2l$ for equilibrium, in which k_1 and k_2 are the bending moment factor [15, 19].

Similar to the previously analysed cases, in the balanced case, the first four constants included in the peel stress expressions are obtained as the solution of the following linear equation set:

$$\begin{aligned}
&\sum_{n=1}^{4} F_n^{\mathrm{B}} \frac{1}{\lambda_n^{\mathrm{B}}} = -F_{12}^{\mathrm{B}}, \\
&\sum_{n=1}^{4} F_n^{\mathrm{B}} \frac{1}{\left(\lambda_n^{\mathrm{B}}\right)^2} = -k_1 h_2 P_0, \\
&\sum_{n=1}^{4} F_n^{\mathrm{B}} \frac{\exp\left(2l\lambda_n^{\mathrm{B}}\right)}{\lambda_n^{\mathrm{B}}} = -F_9^{\mathrm{B}}, \\
&\sum_{n=1}^{4} F_n^{\mathrm{B}} \frac{\exp\left(2l\lambda_n^{\mathrm{B}}\right)}{\left(\lambda_n^{\mathrm{B}}\right)^2} = -k_2 h_1 P_0;
\end{aligned} \tag{23}$$

while the two constants involved in the shear stress expression are:

$$F_5^{\mathrm{B}} = \frac{\lambda_5^{\mathrm{B}}\left(e^{-2l\lambda_5^{\mathrm{B}}} F_{11}^{\mathrm{B}} - F_8^{\mathrm{B}} - 2lF_7^{\mathrm{B}}\right)}{2\cosh\left(2l\lambda_5^{\mathrm{B}}\right)}, \quad F_6^{\mathrm{B}} = \frac{\lambda_5^{\mathrm{B}}\left(e^{2l\lambda_5^{\mathrm{B}}} F_{11}^{\mathrm{B}} - F_8^{\mathrm{B}} - 2lF_7^{\mathrm{B}}\right)}{2\cosh\left(2l\lambda_5^{\mathrm{B}}\right)}. \tag{24}$$

In the unbalanced case, the first six constants are obtained as the solution of the following linear equation set:

$$\begin{aligned}
&\sum_{n=1}^{6} F_n^{\mathrm{U}} \frac{1}{\lambda_n^{\mathrm{U}}} = -F_{12}^{\mathrm{U}}, \\
&\sum_{n=1}^{6} F_n^{\mathrm{U}} \frac{1}{\left(\lambda_n^{\mathrm{U}}\right)^2} = -\frac{F_{11}^{\mathrm{U}} + d_1 M_1}{d_1 + d_2}, \\
&\sum_{n=1}^{6} F_n^{\mathrm{U}} \left[\frac{\left(\lambda_n^{\mathrm{U}}\right)^2}{k_\sigma} - \left(c_1 + c_2\right)\right] = d_1 M_1, \\
&\sum_{n=1}^{6} F_n^{\mathrm{U}} \frac{\exp\left(2l\lambda_n^{\mathrm{U}}\right)}{\lambda_n^{\mathrm{U}}} = -F_9^{\mathrm{U}}, \\
&\sum_{n=1}^{6} F_n^{\mathrm{U}} \frac{\exp\left(2l\lambda_n^{\mathrm{U}}\right)}{\left(\lambda_n^{\mathrm{U}}\right)^2} = -\frac{F_8^{\mathrm{U}} + d_2 M_2 + 2lF_7^{\mathrm{U}}}{d_1 + d_2}, \\
&\sum_{n=1}^{6} F_n^{\mathrm{U}} \left[\frac{\left(\lambda_n^{\mathrm{U}}\right)^2}{k_\sigma} - \left(c_1 + c_2\right)\right] \exp\left(2l\lambda_n^{\mathrm{U}}\right) = d_2 M_2.
\end{aligned} \tag{25}$$

4. Application examples and discussions

To validate the analytic model formulated in this work, we have computed the adhesive peel and shear stresses for some typical adhesively bonded joints subjected to uniform tensile force and/or bending moment. We will show both balanced and unbalanced cases, and compare the results obtained by using the current method with those stemming from other solutions [6, 8] and FEM simulations. For the purpose of comparisons, all of the stress results are given along the mid-plane of the adhesive layer and under a plane strain state. The finite element analysis has been performed by using the commercial code ABAQUS 6.10. In the computational model all of the three layers are assumed to be made of linearly elastic materials, and a plane strain element, CPE4, has been employed. In order to track the potential singular stresses in the near vicinity of the overlap edges, a finer mesh density has been used for such areas. However, close to the middle of the overlap area, where stresses are

almost constant, elements with higher aspect ratios have been used. A magnified view of the FE models in the overlap end region is shown in Fig. 5.

4.1. Balanced adhesively bonded joints

We consider several types of balanced joints, all consisting of two identical adherends made of aluminium, bonded through an adhesive layer. The analytical predictions for the adhesive stresses are obtained by introducing the integration constants, as given by Eqs. (13), (14), (18), (19), (23) and (24), into the stress expressions, Eqs. (8). Material properties are assumed as follows: $E_1 = E_2 = 70$ GPa, $\nu_1 = \nu_2 = 0.34$, $E_a = 2.5$ GPa, $\nu_a = 0.25$. Geometrical dimensions are $H_1 = H_2 = 5$ mm, $h_a = 0.25$ mm, and $2l = 50$ mm.

4.1.1. Stiffened plate/joint

For a balanced stiffened plate/joint, Fig. 6 shows the normalized adhesive stresses as functions of the normalized distance from the symmetry axis. Good agreements between our analytical predictions and the numerical (FEM) results are obtained for both the peel and shear stresses. However, the models proposed in the literature show some discrepancies, especially for the peel stress. Peak values of the adhesive stresses are detected at the right-hand end sections of the joint, indicating that a possible fracture of the adhesive layer will initiate from such sections.

4.1.2. Single-strap joint

For a balanced single-strap joint, Fig. 7 shows the normalized adhesive stresses as functions of the normalized distance from the symmetry axis. A comparison of the different methods indicates that the current model is capable of predicting very accurately the trends of both the peel and shear stresses along the mid-plane of the adhesive layer. The predictions of the models of the literature qualitatively agree with those of the FEM, but are quantitatively inaccurate especially for peel stresses. Very high adhesive stress levels exist close to the interior edge of the bondline, indicating this section as the candidate for the onset of fracture in the adhesive layer.

4.1.3. Single-lap joint

Lastly, we consider a single-lap joint where the adherends are subjected to a tensile load, P_0. Furthermore, to satisfy the static equilibrium conditions additional bending moments and/or transverse shear loads equivalent to a couple $P_0(h_1+h_2)$ must be applied to the structure [11, 12, 15, 16, 19]. For example, if the structure is loaded through pin connections, then nonzero shear forces and zero bending moments at the pins should be introduced

[7]. In the example considered, the equilibrium condition is satisfied by applying both bending moments and transverse shear loads at the end sections of the structure. The bending moment factors $k_1 = \zeta_2 / (\zeta_1 + 2\zeta_1\zeta_2 l + \zeta_2)$ and $k_2 = \zeta_1 / (\zeta_1 + 2\zeta_1\zeta_2 l + \zeta_2)$, in which $\zeta_1 = \sqrt{P_0/D_1}$ and $\zeta_2 = \sqrt{P_0/D_2}$ [19]. Needless to say, the results will be dependent on the secondary loads applied to the structure to maintain its static equilibrium. Fig. 8 shows the normalized adhesive stresses as functions of the normalized distance from the left hand end section. Very high adhesive stresses are predicted at both ends of the overlap, hence adhesive fracture is expected to start from one of such regions. As far as comparisons are concerned, obviously, the present solutions are in good agreement with the FEM results for both peel and shear stresses. Additionally, the predictions from Zou et al. agree well with FEM for shear stresses as well, but some little deviations for the evaluations of peel stress. However, it seems that the classical results from Tsai et al. have more clear deviations compared with FEM.

4.2. Unbalanced adhesively bonded joints

For the unbalanced adhesively bonded joints, the present analytical solution is dependent on determining the integration constants from Eqs. (15), (20), and (25). As an example, we consider some steel-aluminium joints having the following material properties: E_1 = 200GPa, v_1 = 0.29 (steel), E_2 = 70GPa, v_2 = 0.34 (aluminium), and E_a = 2.5GPa, v_a = 0.25 (adhesive). Geometrical dimensions are H_2 = 5mm, h_a = 0.25mm, and $2l$ = 50mm. For the analytical model, we consider three values of the adherends' thickness ratio, H_1 / H_2, namely 0.2, 0.5, and 1. Nevertheless, FEM simulations have been carried out only for H_1 / H_2 = 0.2 to shorten the amount of calculations.

4.2.1. Stiffened plate/joint

Fig. 9 shows the normalized adhesive stresses as functions of the normalized distance from the symmetry axis for an unbalanced stiffened plate/joint under bending moment at three values of the adherends' thickness ratio. Analytical predictions and numerical results match fairly well not only as regards their trends but also from a quantitative viewpoint. Concerning the effects of the thickness ratio, it is observed that the peel stress concentration at the edge of the overlap becomes more severe with the increase of the adherends' thickness ratio. The peak shear stress, however, experiences smaller variations. Such results suggest that designers should focus their attentions not only on increasing the thickness of the cover layer to enhance the overall bending stiffness, but also on preventing the cracking of the adhesive at the edge of the overlap.

4.2.2. Single-strap joint

Fig. 10 shows the normalized adhesive stresses as functions of the normalized distance from the symmetry axis for an unbalanced single-strap joint under tension at three values of the adherends' thickness ratio. Like in the balanced case, both the peel and shear adhesive stresses attain very high peak values at the interior edges of the overlap. Such peak values are much higher than those of at the exterior edges due to the existence of a bending moment at the mid-span. Furthermore, the peak values of the peel stresses are much severe than those of the shear stresses for all the thickness ratios under examination. Adhesive cracking at the mid-span section is therefore expected to be the main failure mode for single-strap joints. Such failure mode could indeed be avoided by using double-sided strap joints to eliminate the parasite bending moment. Concerning the effects of the thickness ratio, we observe that larger values of H_1 / H_2 lead to lower stress concentrations. This effects is related to the higher bending stiffness of the cover layer. In conclusion, stiffer and thicker cover layers are favourable to enhance mechanical durability of single-strap joints.

4.2.3. Single-lap joint

Lastly, we consider an unbalanced single-lap joint under tension. Fig. 11 shows the normalized adhesive stresses as functions of the normalized distance from the left hand end section. The predictions of the current analytical model are in very good agreement with the FEM results. Peak values of both the peel and shear adhesive stresses are detected at the end sections of the adhesive layer. At smaller thickness ratios, because adherend 1 has smaller bending stiffness than adherend 2, the peak values of the adhesive peel stress at $x = 0$ are greater than those at $x = 2l$. This situation may be prevented as increase of the thickness ratio as well as the shear stresses, however, the effect on the right end is not notable.

4.3 Discussion of results

In almost all the above examined cases, an accurate comparison of results shows that the peak values of the peel and shear adhesive stresses are slightly overestimated by the analytical model. Such peak values are always detected at the end points of the overlap region in both the balanced and unbalanced joints. This is inherent in the assumptions underlying the mechanical model, where the adherends are treaded as elastic beams and the adhesive is assumed to be a continuous distribution of uncoupled tension-shear springs. Consequently, the kernels of the related integral equations have only logarithmic singularities and the adhesive stresses are bounded everywhere, including the end sections. In this sense, the boundary condition imposing that the shear stress be zero at the end sections of the overlap region, used in some investigations, is not consistent with the tension-shear spring adhesive model adopted here. This explains also why the overestimation of the analytical

model is higher for shear stresses than for peel stresses.

Like most analytical models available in the literature, the current solution strategy may be unable to accurately predict the stress singularity at the free edges of the overlap region. However, the very good, qualitative and quantitative, agreement of the analytical predictions with the numerical results confirms the validity and reasonable accuracy of the present model. In addition, the process for solving the linear equation sets to obtain the integration constants involved in the stress expressions can be performed conveniently by using any commercial mathematical software tool. Obviously, this solution strategy is more efficient if compared to FEM in order to conduct parametric studies as well as for scaling analysis, design and optimisation of adhesively bonded joints, since it only requires the input of material properties, basic dimensions and external loads. As an application, the failure load predictions for a single-lap joint are implemented and compared with some experimental results as well from Refs. 21, 25 and 26 involving different overlap lengths and adhesive thicknesses, which has been insert into Appendix B.

5. Conclusions

An analytical solution strategy is developed to describe both the balanced and unbalanced adhesively joints subjected to general/mixed force and displacement boundary conditions, and the analytical stress formulas are obtained with identical or different materials. The analytical predictions agree well with the numerical results, not only with regard to their trends but also from the quantitative point of view. The current solution strategy is efficient and reasonably accurate. Thus, it can be used with a certain degree of confidence, in particular for the linear elastic analysis of adhesively bonded joints with relatively small adhesive thickness. This solution is relevant in many practical applications and can help to shed light on the underlying mechanical phenomena, which, therefore, can be considered as a unified engineering tool for the design, structural optimisation and evaluation of adhesive joints.

On the other hand, the analytical formalism developed in this work can be conveniently generalized to a variety of bonded structures and layered structures, such as electronic packaging and flexible electronics structures, where it is technically desired to accurately predict the adhesive stresses and energy release rate to understand the mechanisms of damage evolution and failure [35, 36]. We will apply the proposed methodology to derive design rules for the chip peeling from the adhesive tapes in pick-up process of advanced integrated circuit (IC) packages in future research.

Acknowledgments

The authors acknowledge the Natural Science Foundation of China (51035002, 51175209, 51121002) and New Century Excellent Talents in University (NCET-11-0171) for huge support.

Appendix A

A.1. Internal force and displacement expressions

Here, we present the general expressions for the internal forces and displacements in the adherends. In the balanced case, the axial forces are:

$$\begin{aligned} N_1^{\mathrm{B}}(x) &= -\left[\sum_{n=5}^{6} F_n^{\mathrm{B}} \frac{\exp\left(\lambda_n^{\mathrm{B}} x\right)}{\lambda_n^{\mathrm{B}}} + F_7^{\mathrm{B}} x + F_8^{\mathrm{B}}\right], \\ N_2^{\mathrm{B}}(x) &= \sum_{n=5}^{6} F_n^{\mathrm{B}} \frac{\exp\left(\lambda_n^{\mathrm{B}} x\right)}{\lambda_n^{\mathrm{B}}} + F_7^{\mathrm{B}} x + F_{11}^{\mathrm{B}}; \end{aligned} \tag{A.1}$$

the shear forces are:

$$\begin{aligned} Q_1^{\mathrm{B}}(x) &= -\left[\sum_{n=1}^{4} F_n^{\mathrm{B}} \frac{1}{\lambda_n^{\mathrm{B}}} \exp\left(\lambda_n^{\mathrm{B}} x\right) + F_9^{\mathrm{B}}\right], \\ Q_2^{\mathrm{B}}(x) &= \sum_{n=1}^{4} F_n^{\mathrm{B}} \frac{1}{\lambda_n^{\mathrm{B}}} \exp\left(\lambda_n^{\mathrm{B}} x\right) + F_{12}^{\mathrm{B}}; \end{aligned} \tag{A.2}$$

lastly, the bending moments are:

$$\begin{aligned} M_1^{\mathrm{B}}(x) &= -\left[\sum_{n=1}^{4} F_n^{\mathrm{B}} \frac{1}{\left(\lambda_n^{\mathrm{B}}\right)^2} \exp\left(\lambda_n^{\mathrm{B}} x\right) + h_1 \sum_{n=5}^{6} F_n^{\mathrm{B}} \frac{1}{\lambda_n^{\mathrm{B}}} \exp\left(\lambda_n^{\mathrm{B}} x\right) + \left(F_9^{\mathrm{B}} + h_1 F_7^{\mathrm{B}}\right) x + F_{10}^{\mathrm{B}}\right], \\ M_2^{\mathrm{B}}(x) &= \sum_{n=1}^{4} F_n^{\mathrm{B}} \frac{1}{\left(\lambda_n^{\mathrm{B}}\right)^2} \exp\left(\lambda_n^{\mathrm{B}} x\right) - h_2 \sum_{n=5}^{6} F_n^{\mathrm{B}} \frac{1}{\lambda_n^{\mathrm{B}}} \exp\left(\lambda_n^{\mathrm{B}} x\right) + \left(F_{12}^{\mathrm{B}} - h_2 F_7^{\mathrm{B}}\right) x + F_{13}^{\mathrm{B}}; \end{aligned} \tag{A.3}$$

where F_8^{B}, F_9^{B}, …, F_{13}^{B} are integration constants.

The internal forc expressions e, Eqs. (A.1) - (A.3), are substituted into Eq. (4). Then, by integrating the latter with respect to *x*, the expressions for the displacements are also derived. The mid-plane axial displacements are:

$$\begin{aligned} u_1^{\mathrm{B}}(x) &= -a_1\left[\sum_{n=5}^{6} F_n^{\mathrm{B}} \frac{1}{\left(\lambda_n^{\mathrm{B}}\right)^2} \exp\left(\lambda_n^{\mathrm{B}} x\right) + \frac{1}{2} F_7^{\mathrm{B}} x^2 + F_8^{\mathrm{B}} x + F_{14}^{\mathrm{B}}\right], \\ u_2^{\mathrm{B}}(x) &= a_2\left[\sum_{n=5}^{6} F_n^{\mathrm{B}} \frac{1}{\left(\lambda_n^{\mathrm{B}}\right)^2} \exp\left(\lambda_n^{\mathrm{B}} x\right) + \frac{1}{2} F_7^{\mathrm{B}} x^2 + F_{11}^{\mathrm{B}} x + F_{17}^{\mathrm{B}}\right]; \end{aligned} \tag{A.4}$$

the rotations of the cross sections are:

$$\begin{aligned} \phi_1^{\mathrm{B}}(x) &= -d_1\left[\sum_{n=1}^{4} F_n^{\mathrm{B}} \frac{1}{\left(\lambda_n^{\mathrm{B}}\right)^3} \exp\left(\lambda_n^{\mathrm{B}} x\right) + h_1 \sum_{n=5}^{6} F_n^{\mathrm{B}} \frac{1}{\left(\lambda_n^{\mathrm{B}}\right)^2} \exp\left(\lambda_n^{\mathrm{B}} x\right) + \frac{1}{2}\left(F_9^{\mathrm{B}} + h_1 F_7^{\mathrm{B}}\right) x^2 + F_{10}^{\mathrm{B}} x + F_{15}^{\mathrm{B}}\right], \\ \phi_2^{\mathrm{B}}(x) &= d_2\left[\sum_{n=1}^{4} F_n^{\mathrm{B}} \frac{1}{\left(\lambda_n^{\mathrm{B}}\right)^3} \exp\left(\lambda_n^{\mathrm{B}} x\right) - h_2 \sum_{n=5}^{6} F_n^{\mathrm{B}} \frac{1}{\left(\lambda_n^{\mathrm{B}}\right)^2} \exp\left(\lambda_n^{\mathrm{B}} x\right) + \frac{1}{2}\left(F_{12}^{\mathrm{B}} - h_2 F_7^{\mathrm{B}}\right) x^2 + F_{13}^{\mathrm{B}} x + F_{18}^{\mathrm{B}}\right]; \end{aligned} \tag{A.5}$$

lastly, the mid-plane transverse displacements are:

$$
\begin{aligned}
w_1^{\mathrm{B}}(x) &= \sum_{n=1}^{4} F_n^{\mathrm{B}} \left[\frac{d_1}{\left(\lambda_n^{\mathrm{B}}\right)^4} - \frac{c_1}{\left(\lambda_n^{\mathrm{B}}\right)^2} \right] \exp\left(\lambda_n^{\mathrm{B}} x\right) + d_1 h_1 \sum_{n=5}^{6} F_n^{\mathrm{B}} \frac{1}{\left(\lambda_n^{\mathrm{B}}\right)^3} \exp\left(\lambda_n^{\mathrm{B}} x\right) + \frac{1}{6}\left(d_1 F_9^{\mathrm{B}} + d_1 h_1 F_7^{\mathrm{B}}\right) x^3 + \frac{1}{2} d_1 F_{10}^{\mathrm{B}} x^2 + \left(d_1 F_{15}^{\mathrm{B}} - c_1 F_9^{\mathrm{B}}\right) x + F_{16}^{\mathrm{B}}, \\
w_2^{\mathrm{B}}(x) &= \sum_{n=1}^{4} F_n^{\mathrm{B}} \left[\frac{c_2}{\left(\lambda_n^{\mathrm{B}}\right)^2} - \frac{d_2}{\left(\lambda_n^{\mathrm{B}}\right)^4} \right] \exp\left(\lambda_n^{\mathrm{B}} x\right) + d_2 h_2 \sum_{n=5}^{6} F_n^{\mathrm{B}} \frac{1}{\left(\lambda_n^{\mathrm{B}}\right)^3} \exp\left(\lambda_n^{\mathrm{B}} x\right) - \frac{1}{6}\left(d_2 F_{12}^{\mathrm{B}} - d_2 h_2 F_7^{\mathrm{B}}\right) x^3 - \frac{1}{2} d_2 F_{13}^{\mathrm{B}} x^2 + \left(c_2 F_{12}^{\mathrm{B}} - d_2 F_{18}^{\mathrm{B}}\right) x + F_{19}^{\mathrm{B}};
\end{aligned}
\tag{A.6}
$$

where F_{14}^{B}, F_{15}^{B}, …, F_{19}^{B} are further integration constants. All such constants are to be determined by imposing the boundary conditions.

In the same way we derive the analytical expressions for the internal forces and displacements in the unbalanced case. The axial forces are:

$$
\begin{aligned}
N_1^{\mathrm{U}}(x) &= \frac{1}{d_1 h_1 - d_2 h_2} \left\{ \sum_{n=1}^{6} F_n^{\mathrm{U}} \left[\frac{\left(\lambda_n^{\mathrm{U}}\right)^2}{k_\sigma} - \left(c_1 + c_2\right) + \frac{d_1 + d_2}{\left(\lambda_n^{\mathrm{U}}\right)^2} \right] \exp\left(\lambda_n^{\mathrm{U}} x\right) + F_7^{\mathrm{U}} x + F_8^{\mathrm{U}} \right\}, \\
N_2^{\mathrm{U}}(x) &= -\frac{1}{d_1 h_1 - d_2 h_2} \left\{ \sum_{n=1}^{6} F_n^{\mathrm{U}} \left[\frac{\left(\lambda_n^{\mathrm{U}}\right)^2}{k_\sigma} - \left(c_1 + c_2\right) + \frac{d_1 + d_2}{\left(\lambda_n^{\mathrm{U}}\right)^2} \right] \exp\left(\lambda_n^{\mathrm{U}} x\right) + F_7^{\mathrm{U}} x + F_{11}^{\mathrm{U}} \right\};
\end{aligned}
\tag{A.7}
$$

the shear forces are:

$$
\begin{aligned}
Q_1^{\mathrm{U}}(x) &= -\left[\sum_{n=1}^{6} F_n^{\mathrm{U}} \frac{1}{\lambda_n^{\mathrm{Ub}}} \exp\left(\lambda_n^{\mathrm{U}} x\right) + F_9^{\mathrm{U}} \right], \\
Q_2^{\mathrm{U}}(x) &= \sum_{n=1}^{6} F_n^{\mathrm{U}} \frac{1}{\lambda_n^{\mathrm{U}}} \exp\left(\lambda_n^{\mathrm{U}} x\right) + F_{12}^{\mathrm{U}};
\end{aligned}
\tag{A.8}
$$

the bending moments are:

$$
\begin{aligned}
M_1^{\mathrm{U}}(x) &= \frac{h_1}{d_1 h_1 - d_2 h_2} \left\{ \sum_{n=1}^{6} F_n^{\mathrm{U}} \left[\frac{\left(\lambda_n^{\mathrm{U}}\right)^2}{k_\sigma} - \left(c_1 + c_2\right) + \frac{d_2\left(h_1 + h_2\right)}{h_1\left(\lambda_n^{\mathrm{U}}\right)^2} \right] \exp\left(\lambda_n^{\mathrm{U}} x\right) + \left(F_7^{\mathrm{U}} - \frac{d_1 h_1 - d_2 h_2}{h_1} F_9^{\mathrm{U}} \right) x + F_{10}^{\mathrm{U}} \right\}, \\
M_2^{\mathrm{U}}(x) &= \frac{h_2}{d_1 h_1 - d_2 h_2} \left\{ \sum_{n=1}^{6} F_n^{\mathrm{U}} \left[\frac{\left(\lambda_n^{\mathrm{U}}\right)^2}{k_\sigma} - \left(c_1 + c_2\right) + \frac{d_1\left(h_1 + h_2\right)}{h_2\left(\lambda_n^{\mathrm{U}}\right)^2} \right] \exp\left(\lambda_n^{\mathrm{U}} x\right) + \left(F_7^{\mathrm{U}} + \frac{d_1 h_1 - d_2 h_2}{h_2} F_{12}^{\mathrm{U}} \right) x + F_{13}^{\mathrm{U}} \right\};
\end{aligned}
\tag{A.9}
$$

Furthermore, the mid-plane axial displacements are:

$$
\begin{aligned}
u_1^{\mathrm{U}}(x) &= \frac{a_1}{d_1 h_1 - d_2 h_2} \left\{ \sum_{n=1}^{6} F_n^{\mathrm{U}} \left[\frac{\lambda_n^{\mathrm{U}}}{k_\sigma} - \frac{c_1 + c_2}{\lambda_n^{\mathrm{U}}} + \frac{d_1 + d_2}{\left(\lambda_n^{\mathrm{U}}\right)^3} \right] \exp\left(\lambda_n^{\mathrm{U}} x\right) + \frac{1}{2} F_7^{\mathrm{U}} x^2 + F_8^{\mathrm{U}} x + F_{14}^{\mathrm{U}} \right\}, \\
u_2^{\mathrm{U}}(x) &= -\frac{a_2}{d_1 h_1 - d_2 h_2} \left\{ \sum_{n=1}^{6} F_n^{\mathrm{U}} \left[\frac{\lambda_n^{\mathrm{U}}}{k_\sigma} - \frac{c_1 + c_2}{\lambda_n^{\mathrm{U}}} + \frac{d_1 + d_2}{\left(\lambda_n^{\mathrm{U}}\right)^3} \right] \exp\left(\lambda_n^{\mathrm{U}} x\right) + \frac{1}{2} F_7^{\mathrm{U}} x^2 + F_{11}^{\mathrm{U}} x + F_{17}^{\mathrm{U}} \right\};
\end{aligned}
\tag{A.10}
$$

the rotations of the cross sections are:

$$
\begin{aligned}
\phi_1^{\mathrm{U}}(x) &= \frac{d_1 h_1}{d_1 h_1 - d_2 h_2} \left\{ \sum_{n=1}^{6} F_n^{\mathrm{U}} \left[\frac{\lambda_n^{\mathrm{U}}}{k_\sigma} - \frac{c_1 + c_2}{\lambda_n^{\mathrm{U}}} + \frac{d_2\left(h_1 + h_2\right)}{h_1\left(\lambda_n^{\mathrm{U}}\right)^3} \right] \exp\left(\lambda_n^{\mathrm{U}} x\right) + \frac{1}{2}\left(F_7^{\mathrm{U}} - \frac{d_1 h_1 - d_2 h_2}{h_1} F_9^{\mathrm{U}} \right) x^2 + F_{10}^{\mathrm{U}} x + F_{15}^{\mathrm{U}} \right\}, \\
\phi_2^{\mathrm{U}}(x) &= \frac{d_2 h_2}{d_1 h_1 - d_2 h_2} \left\{ \sum_{n=1}^{6} F_n^{\mathrm{U}} \left[\frac{\lambda_n^{\mathrm{U}}}{k_\sigma} - \frac{c_1 + c_2}{\lambda_n^{\mathrm{U}}} + \frac{d_1\left(h_1 + h_2\right)}{h_2\left(\lambda_n^{\mathrm{U}}\right)^3} \right] \exp\left(\lambda_n^{\mathrm{U}} x\right) + \frac{1}{2}\left(F_7^{\mathrm{U}} + \frac{d_1 h_1 - d_2 h_2}{h_2} F_{12}^{\mathrm{U}} \right) x^2 + F_{13}^{\mathrm{U}} x + F_{18}^{\mathrm{U}} \right\};
\end{aligned}
\tag{A.11}
$$

lastly, the mid-plane transverse displacements are:

$$
\begin{aligned}
w_1^{\mathrm{U}}(x) = &-\frac{1}{d_1h_1 - d_2h_2}\left\{\begin{array}{l}\displaystyle\sum_{n=1}^{6} F_n^{\mathrm{U}}\left[\frac{d_1h_1}{k_\sigma} - \frac{d_2h_2c_1 + d_1h_1c_2}{\left(\lambda_n^{\mathrm{U}}\right)^2} + \frac{d_1d_2\left(h_1+h_2\right)}{\left(\lambda_n^{\mathrm{U}}\right)^4}\right]\exp\left(\lambda_n^{\mathrm{U}}x\right) \\ +\frac{1}{6}\left[d_1h_1F_7^{\mathrm{U}} - d_1F_9^{\mathrm{U}}\left(d_1h_1 - d_2h_2\right)\right]x^3 + \frac{1}{2}d_1h_1F_{10}^{\mathrm{U}}x^2 + \left[d_1h_1F_{15}^{\mathrm{U}} + c_1F_9^{\mathrm{U}}\left(d_1h_1 - d_2h_2\right)\right]x + F_{16}^{\mathrm{U}}\end{array}\right\}, \\
w_2^{\mathrm{U}}(x) = &-\frac{1}{d_1h_1 - d_2h_2}\left\{\begin{array}{l}\displaystyle\sum_{n=1}^{6} F_n^{\mathrm{U}}\left[\frac{d_2h_2}{k_\sigma} - \frac{d_2h_2c_1 + d_1h_1c_2}{\left(\lambda_n^{\mathrm{U}}\right)^2} + \frac{d_1d_2\left(h_1+h_2\right)}{\left(\lambda_n^{\mathrm{U}}\right)^4}\right]\exp\left(\lambda_n^{\mathrm{U}}x\right) \\ +\frac{1}{6}\left[d_2h_2F_7^{\mathrm{U}} + d_2F_{12}^{\mathrm{U}}\left(d_1h_1 - d_2h_2\right)\right]x^3 + \frac{1}{2}d_2h_2F_{13}^{\mathrm{U}}x^2 + \left[d_2h_2F_{18}^{\mathrm{U}} - c_2F_{12}^{\mathrm{U}}\left(d_1h_1 - d_2h_2\right)\right]x + F_{19}^{\mathrm{U}}\end{array}\right\};
\end{aligned}
\tag{A.12}
$$

where F_8^{U}, F_9^{U}, ..., F_{19}^{U} are integration constants.

A.2. Relationships among the integration constants

The integration constants are not independent of each other. Indeed, by introducing the expressions for the adhesive stresses and displacements into Eq. (2), we obtain the following relationships:

$$
\begin{aligned}
&d_1F_9^{\mathrm{B}} + d_2F_{12}^{\mathrm{B}} = 0, \\
&d_1F_{10}^{\mathrm{B}} + d_2F_{13}^{\mathrm{B}} = 0, \\
&c_1F_9^{\mathrm{B}} + c_2F_{12}^{\mathrm{B}} - d_1F_{15}^{\mathrm{B}} - d_2F_{18}^{\mathrm{B}} = 0, \\
&d_1h_1F_9^{\mathrm{B}} - d_2h_2F_{12}^{\mathrm{B}} + \left(a_1 + a_2 + d_1h_1^2 + d_2h_2^2\right)F_7^{\mathrm{B}} = 0, \\
&a_1F_8^{\mathrm{B}} + a_2F_{11}^{\mathrm{B}} + d_1h_1F_{10}^{\mathrm{B}} - d_2h_2F_{13}^{\mathrm{B}} = 0, \\
&a_1F_{14}^{\mathrm{B}} + a_2F_{17}^{\mathrm{B}} + d_1h_1F_{15}^{\mathrm{B}} - d_2h_2F_{18}^{\mathrm{B}} - F_7^{\mathrm{B}}/k_\tau = 0, \\
&F_{16}^{\mathrm{B}} - F_{19}^{\mathrm{B}} = 0,
\end{aligned}
\tag{A.13}
$$

for the balanced case; and:

$$
\begin{aligned}
&F_7^{\mathrm{U}} - \left(d_1F_9^{\mathrm{U}} + d_2F_{12}^{\mathrm{U}}\right) = 0, \\
&d_1h_1F_{10}^{\mathrm{U}} - d_2h_2F_{13}^{\mathrm{U}} = 0, \\
&\left(d_1h_1 - d_2h_2\right)\left(c_1F_9^{\mathrm{U}} + c_2F_{12}^{\mathrm{U}}\right) + \left(d_1h_1F_{15}^{\mathrm{U}} - d_2h_2F_{18}^{\mathrm{U}}\right) = 0, \\
&\left(a_1 + a_2 + d_1h_1^2 + d_2h_2^2\right)F_7^{\mathrm{U}} - \left(d_1h_1 - d_2h_2\right)\left(d_1h_1F_9^{\mathrm{U}} - d_2h_2F_{12}^{\mathrm{U}}\right) = 0, \\
&a_1F_8^{\mathrm{U}} + a_2F_{11}^{\mathrm{U}} + d_1h_1^2F_{10}^{\mathrm{U}} + d_2h_2^2F_{13}^{\mathrm{U}} = 0, \\
&a_1F_{14}^{\mathrm{U}} + a_2F_{17}^{\mathrm{U}} + d_1h_1^2F_{15}^{\mathrm{U}} + d_2h_2^2F_{18}^{\mathrm{U}} - F_7^{\mathrm{U}}/k_\tau = 0, \\
&F_{16}^{\mathrm{U}} - F_{19}^{\mathrm{U}} = 0,
\end{aligned}
\tag{A.14}
$$

for the unbalanced case.

A.3. Integration constants

By introducing the expressions for the internal forces and displacements into the suitable boundary conditions, holding for any particular type of adhesively bonded joint, we obtain the values of the integration constants. For stiffened and single-strap joints in this paper, we find that the constants F_7^{B}, F_9^{B} and F_{12}^{B} of the balanced case as well as F_7^{U}, F_9^{U} and F_{12}^{U} of the unbalanced case are equal to zero. For a general single-lap joint, however, they can be written as:

$$
\begin{aligned}
F_7^{\mathrm{B}} &= \frac{d_1 d_2 \left(h_1 + h_2\right)}{\left(d_1 + d_2\right)\left(a_1 + a_2 + d_1 h_1^2 + d_2 h_2^2\right)} Q_0, \\
F_9^{\mathrm{B}} &= -\frac{d_2}{d_1 + d_2} Q_0, \\
F_{12}^{\mathrm{B}} &= \frac{d_1}{d_1 + d_2} Q_0,
\end{aligned}
\tag{A.15}
$$

for a balanced case and for an unbalanced case:

$$
\begin{aligned}
F_7^{\mathrm{U}} &= -\frac{d_1 d_2 \left(h_1 + h_2\right)\left(d_1 h_1 - d_2 h_2\right)}{\left(a_1 + a_2\right)\left(d_1 + d_2\right) + d_1 d_2 \left(h_1 + h_2\right)^2} Q_0, \\
F_9^{\mathrm{U}} &= -\frac{d_2 \left[d_1 h_1 \left(h_1 + h_2\right) + \left(a_1 + a_2\right)\right]}{\left(a_1 + a_2\right)\left(d_1 + d_2\right) + d_1 d_2 \left(h_1 + h_2\right)^2} Q_0, \\
F_{12}^{\mathrm{U}} &= \frac{d_1 \left[d_2 h_2 \left(h_1 + h_2\right) + \left(a_1 + a_2\right)\right]}{\left(a_1 + a_2\right)\left(d_1 + d_2\right) + d_1 d_2 \left(h_1 + h_2\right)^2} Q_0.
\end{aligned}
\tag{A.16}
$$

In addition, the integration constants F_8^{B}, F_{10}^{B}, F_{11}^{B} and F_{13}^{B} have the expressions listed in the following.

For a balanced stiffened plate/joint under tension and/or bending moment:

$$
\begin{aligned}
F_8^{\mathrm{B}} &= -\frac{a_2 \left(d_1 + d_2\right) P_0 + d_1 d_2 \left(h_1 + h_2\right) M_0}{\left(a_1 + a_2\right)\left(d_1 + d_2\right) + d_1 d_2 \left(h_1 + h_2\right)^2}, \\
F_{10}^{\mathrm{B}} &= -\frac{a_2 d_2 \left(h_1 + h_2\right) P_0 - d_2 \left(a_1 + a_2\right) M_0}{\left(a_1 + a_2\right)\left(d_1 + d_2\right) + d_1 d_2 \left(h_1 + h_2\right)^2}, \\
F_{11}^{\mathrm{B}} &= \frac{\left[a_1 \left(d_1 + d_2\right) + d_1 d_2 \left(h_1 + h_2\right)^2\right] P_0 - d_1 d_2 \left(h_1 + h_2\right) M_0}{\left(a_1 + a_2\right)\left(d_1 + d_2\right) + d_1 d_2 \left(h_1 + h_2\right)^2}, \\
F_{13}^{\mathrm{B}} &= \frac{a_2 d_1 \left(h_1 + h_2\right) P_0 - d_1 \left(a_1 + a_2\right) M_0}{\left(a_1 + a_2\right)\left(d_1 + d_2\right) + d_1 d_2 \left(h_1 + h_2\right)^2};
\end{aligned}
\tag{A.17}
$$

for a balanced single-strap joint under tension:

$$
\begin{aligned}
F_8^{\mathrm{B}} &= -\frac{a_2 \left(d_1 + d_2\right)}{\left(a_1 + a_2\right)\left(d_1 + d_2\right) + d_1 d_2 \left(h_1 + h_2\right)^2} P_0, \\
F_{10}^{\mathrm{B}} &= -\frac{a_2 d_2 \left(h_1 + h_2\right)}{\left(a_1 + a_2\right)\left(d_1 + d_2\right) + d_1 d_2 \left(h_1 + h_2\right)^2} P_0, \\
F_{11}^{\mathrm{B}} &= \frac{a_1 \left(d_1 + d_2\right) + d_1 d_2 \left(h_1 + h_2\right)^2}{\left(a_1 + a_2\right)\left(d_1 + d_2\right) + d_1 d_2 \left(h_1 + h_2\right)^2} P_0, \\
F_{13}^{\mathrm{B}} &= \frac{a_2 d_1 \left(h_1 + h_2\right)}{\left(a_1 + a_2\right)\left(d_1 + d_2\right) + d_1 d_2 \left(h_1 + h_2\right)^2} P_0;
\end{aligned}
\tag{A.18}
$$

for a balanced single-lap joint under tension:

$$
\begin{aligned}
F_8^{\mathrm{B}} &= \frac{d_1 d_2 \left(h_1+h_2\right)^2 \left(k_1-1\right) - a_2 \left(d_1+d_2\right)}{\left(a_1+a_2\right)\left(d_1+d_2\right)+d_1 d_2 \left(h_1+h_2\right)^2} P_0, \\
F_{10}^{\mathrm{B}} &= \frac{d_2 \left(h_1+h_2\right)\left(a_1-a_1 k_1-a_2 k_1\right)}{\left(a_1+a_2\right)\left(d_1+d_2\right)+d_1 d_2 \left(h_1+h_2\right)^2} P_0, \\
F_{11}^{\mathrm{B}} &= \frac{a_1 \left(d_1+d_2\right)+d_1 d_2 k_1 \left(h_1+h_2\right)^2}{\left(a_1+a_2\right)\left(d_1+d_2\right)+d_1 d_2 \left(h_1+h_2\right)^2} P_0, \\
F_{13}^{\mathrm{B}} &= \frac{d_1 \left(h_1+h_2\right)\left(a_1 k_1+a_2 k_1-a_1\right)}{\left(a_1+a_2\right)\left(d_1+d_2\right)+d_1 d_2 \left(h_1+h_2\right)^2} P_0.
\end{aligned}
\tag{A.19}
$$

The constants entering the solution for any unbalanced joint can be expressed in terms of the corresponding constants for the balanced case:

$$
\begin{aligned}
F_8^{\mathrm{U}} &= \left(d_2 h_2 - d_1 h_1\right) F_8^{\mathrm{B}}, \\
F_{10}^{\mathrm{U}} &= \frac{d_2 h_2 - d_1 h_1}{h_1} F_{10}^{\mathrm{B}}, \\
F_{11}^{\mathrm{U}} &= \left(d_2 h_2 - d_1 h_1\right) F_{11}^{\mathrm{B}}, \\
F_{13}^{\mathrm{U}} &= \frac{d_1 h_1 - d_2 h_2}{h_2} F_{13}^{\mathrm{B}}.
\end{aligned}
\tag{A.20}
$$

Appendix B: failure load predictions and comparison with experimental results

In this section, the stress expressions (8) combined with the linear equation sets (23) and (24) of the balanced single-lap joint will be used to predict the joint strength, and compared with experimental results. It should be pointed out that the failure criteria used in this paper are based on maximum stress criterion in the adhesive layer, namely the failure occurs when the peak shear or peel stresses reach the strength of the material τ_{r} or σ_{r}. According to Eq. (8), the maximum peel and shear stresses can be written as $\sigma_{\mathrm{B}}\big|_{x=0} = \sum_{n=1}^{4} F_n^{\mathrm{B}}$ and $\tau_{\mathrm{B}}\big|_{x=0} = \sum_{n=5}^{7} F_n^{\mathrm{B}}$. If denoting $f_n^{\mathrm{B}} = F_n^{\mathrm{B}} / P_0$, for a single-lap joint with b width the failure load can be predicted by $P_0 = \sigma_{\mathrm{r}} b \Big/ \sum_{n=1}^{4} f_n^{\mathrm{B}}$ or $P_0 = \tau_{\mathrm{r}} b \Big/ \sum_{n=5}^{7} f_n^{\mathrm{B}}$. All of the geometrical and material properties as well as experimental results are from the Refs. 21, 24 and 25. In addition, the objective here is to assess whether the presented analytical solution can be used to simulate failure loads, with respect to the experimental details and further discussions, we kindly refer the readers to review papers by Adams, da Silva and Karachalios, etc. [21, 25-27].

Fig. 12 presents the effects of overlap length on the joint strength, where the joints are made of brittle adhesive (Redux 326: E = 4.44 GPa, ν = 0.35, σ_{r} = 50.9 MPa, τ_{r} = 36.5 MPa) with the thickness of 0.2 mm and high-strength steel (E = 210 GPa, ν = 0.3) adherends with the thickness of 1.5 mm. The overlaps' lengths are fixed at 12.5, 25 and 50 mm, respectively. Obviously, the linear solutions presented in this paper can track the trends of failure load, even give a good prediction for short overlap. Although all the predictions are lower than

the experimental results, fortunately, this is just a safe design. On the other hand, for the ductile adhesive, such as Hysol 9321, the experimental results show that the joint strength decreases as the bondline gets thicker [26]. The linear solutions, however, present the opposite trend, which implies the fact that linear elastic model ignoring the adhesive nonlinearity may be unsuitable to investigate the effect of adhesive thickness.

References

[1] Akpinar S, Doru MO, Özel A, Aydin MD. Jahanpasand HG, The effect of the spew fillet on an adhesively bonded single-lap joint subjected to bending moment. Compos. Pt. B-Eng. 55 (2013) 55-64.

[2] da Silva LFM, Lopes MJCQ. Joint strength optimization by the mixed-adhesive technique, Int. J. Adhes. Adhes. 29 (2009) 509-14.

[3] Cheng J, Taheri F. A smart single-lap adhesive joint integrated with partially distributed piezoelectric patches. International Int. J. Solids Struct. 43 (2006) 1079-92.

[4] Cheng H, Wu J, Li M, Kim DH, Kim YS, Huang Y, *et al.* An analytical model of strain isolation for stretchable and flexible electronics. Appl. Phys. Lett. 98 (2011) 061902--3.

[5] Jiang ZQ, Huang Y, Chandra A. Thermal Stresses in Layered Electronic Assemblies. J. Electron. Packag. 119 (1997) 127-32.

[6] Wang KP, Huang YY, Chandra A, Hu KX. Interfacial shear stress, peeling stress, and die cracking stress in trilayer electronic assemblies. IEEE Trans. Compon. Pack. Manuf. Technol. 23 (2000) 309-16.

[7] Delale F, Erdogan F, Aydinoglu M. Stresses in adhesively bonded joints: a closed-form solution. J. Compos. Mater. 15 (1981) 249-71.

[8] Zou G, Shahin K, Taheri F. An analytical solution for the analysis of symmetric composite adhesively bonded joints. Compos. Struct. 65(2004) 499-510.

[9] Shahin K, Taheri F. Analysis of deformations and stresses in balanced and unbalanced adhesively bonded single-strap joints. Compos. Struct. 81(2007) 511-24.

[10] Li G. Elastic analysis of closed-form solutions for adhesive stresses in bonded single-strap butt joints. J. Mech. Mater. Struct. 5(2010) 409-26.

[11] Goland M, Reissner E. The stresses in cemented joints. J. Appl. Mech.-Trans. ASME, 11 (1944) A17-A27.

[12] Hart-Smith LJ. Adhesive-bonded single-lap joints. NASA Technical Report. CR-112236 (1973).

[13] Adams RD, Peppiatt N. Stress analysis of adhesive-bonded lap joints. J. Strain Anal. Eng. Des. 9 (1974) 185-96.

[14] Adams RD, Strength predictions for lap joints, especially with composite adherends. A review, J. Adhes., 30 (1989) 219-42.

[15] Cheng S, Chen D, Shi Y. Analysis of Adhesive-Bonded Joints with Nonidentical Adherends. J. Eng. Mech.

117 (1991) 605-23.

[16] Adams RD, Mallick V, A method for the stress analysis of lap joints, J. Adhes., 38 (1992) 199-217.

[17] Tsai MY, Morton J, A note on peel stresses in single-lap adhesive joints, J. Appl. Mech.-Trans. ASME, 61 (1994) 712-5.

[18] Tsai MY, Oplinger DW, Morton J. Improved theoretical solutions for adhesive lap joints. Int. J. Solids Struct. 35 (1998) 1163-85.

[19] Zhao X, Adams RD, da Silva LFM, A new method for the determination of bending moments in single lap joints, Int. J. Adhes. Adhes., 30 (2010) 63-71.

[20] Sayman O, Elasto-plastic stress analysis in an adhesively bonded single-lap joint, Compos. Pt. B-Eng., 43 (2012) 204-9.

[21] da Silva LFM, das Neves PJC, Adams RD, Spelt JK. Analytical models of adhesively bonded joints—Part I: Literature survey. Int. J. Adhes. Adhes. 29 (2009) 319-30.

[22] da Silva LFM, das Neves PJC., Adams RD, Wang A, Spelt JK, Analytical models of adhesively bonded joints—Part II: Comparative study, Int. J. Adhes. Adhes., 29 (2009) 331-41.

[23] He X. A review of finite element analysis of adhesively bonded joints. Int. J. Adhes. Adhes. 31 (2011) 248-264.

[24] Bigwood D, Crocombe A, Elastic analysis and engineering design formulae for bonded joints, Int. J. Adhes. Adhes, 9 (1989) 229-42.

[25] Harris JA, Adams RD, Strength prediction of bonded single lap joints by non-linear finite element methods, Int. J. Adhes. Adhes., 4 (1984) 65-78.

[26] da Silva LFM, Adams RD, Gibbs M, Manufacture of adhesive joints and bulk specimens with high-temperature adhesives, Int. J. Adhes. Adhes., 24 (2004) 69-83.

[27] da Silva LFM, Rodrigues T, Figueiredo M, De Moura M, Chousal J, Effect of adhesive type and thickness on the lap shear strength, J. Adhes., 82 (2006) 1091-115.

[28] Karachalios EF, Adams RD, da Silva LFM, Single lap joints loaded in tension with ductile steel adherends, Int. J. Adhes. Adhes., 43 (2013) 96-108.

[29] Karachalios EF, Adams RD, da Silva LFM, Single lap joints loaded in tension with high strength steel adherends, Int. J. Adhes. Adhes., 43 (2013) 81-95.

[30] Tay T. Characterization and analysis of delamination fracture in composites: an overview of developments from 1990 to 2001. Appl. Mech. Rev. 56 (2003) 1-31.

[31] Bennati S, Colleluori M, Corigliano D, Valvo PS. An enhanced beam-theory model of the asymmetric double cantilever beam (ADCB) test for composite laminates. Compos. Sci. Technol. 9 (2009) 1735-45.

[32] Bennati S, Fisicaro P, Valvo P. An enhanced beam-theory model of the mixed-mode bending (MMB) test—Part I: Literature review and mechanical model. Meccanica. 48 (2013) 443-62.

[33] Bennati S, Fisicaro P, Valvo P. An enhanced beam-theory model of the mixed-mode bending (MMB) test—Part II: Applications and results. Meccanica. 48 (2013) 465-84.

[34] Bennati S, Taglialegne L, Valvo PS. Modelling of interfacial fracture of layered structures. Proc. 18th European Conference on Fracture: Fracture of Materials and Structures from Micro to Macro Scale, ECF 2010, Dresden, Germany, August 30–September 3.

[35] Liu Z, Valvo PS, Huang Y, Yin Z. Cohesive failure analysis of an array of IC chips bonded to a stretched substrate. Int. J. Solids Struct. 50 (2013) 3528-38.

[36] Liu Z, Huang Y, Chen J, Yin Z, Tunable peeling technique and mechanism of thin chip from compliant

adhesive tapes, IEEE Trans. Compon. Pack. Manuf. Technol., 4 (2014) 560-568.

Figure Captions:

Fig. 1. (a) Typical adhesively bonded joints and corresponding overlap region; (b) free-body diagrams of adherend and adhesive infinitesimal elements.

Fig. 2. (a) A stiffened plate joint under axial tension and bending moment; (b) reduced right-hand half portion of the joint.

Fig. 3. (a) A single-strap joint under axial tensile loading; (b) reduced right-hand half portion of the joint.

Fig. 4. (a) A single-lap joint under axial tensile loading; (b) schematic overlap area with boundary forces.

Fig. 5. Detailed 2D finite element mesh

Fig. 6. Normalized adhesive stresses for a balanced stiffened plate joint under bending: (a) peel stresses; (b) shear stresses.

Fig.7. Normalized adhesive stresses for a balanced single-strap joint under tension: (a) peel stresses; (b) shear stresses.

Fig. 8. Normalized adhesive stresses for a balanced single-lap joint under tension: (a) peel stresses; (b) shear stresses.

Fig. 9. Normalized adhesive stresses for an unbalanced stiffened plate joint under bending: (a) peel stresses; (b) shear stresses.

Fig. 10. Normalized adhesive stresses for an unbalanced single-strap joint under tension: (a) peel stresses; (b) shear stresses.

Fig. 11. Normalized adhesive stresses for an unbalanced single-lap joint under tension: (a) peel stresses; (b) shear stresses.

Fig. 12. Verification of the prediction of failure load considering the brittle adhesive (Redux 326) for 12.5, 25 and 50 mm overlap lengths. The experimental data are from Refs. 21 and 25.

Figures

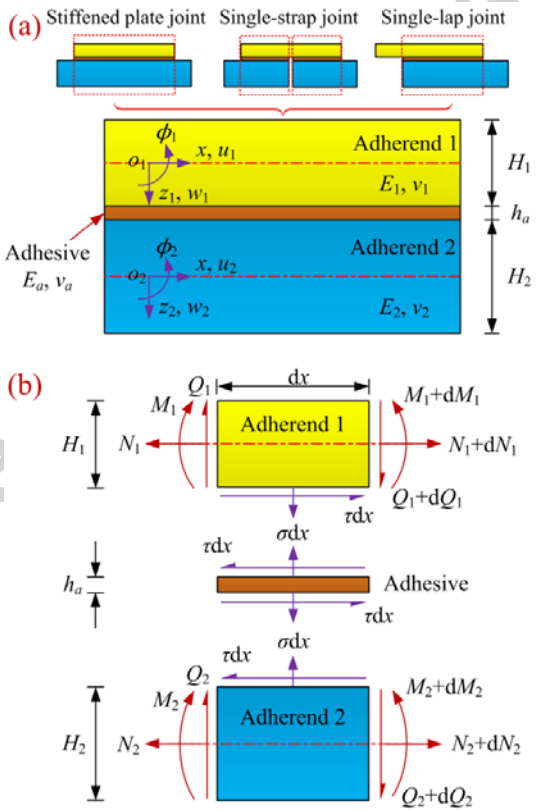

Fig. 1. (a) Typical adhesively bonded joints and corresponding overlap region; (b) free-body diagrams of adherend and adhesive infinitesimal elements.

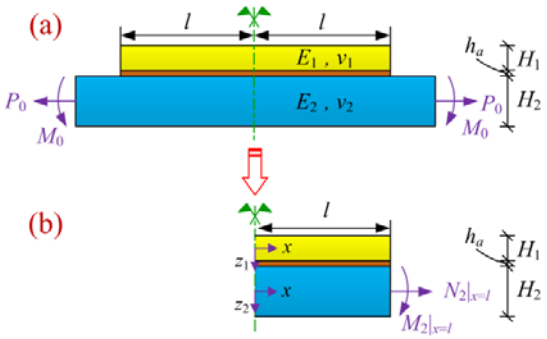

Fig. 2. (a) A stiffened plate/joint under axial tension and bending moment; (b) reduced right-hand half portion of the joint.

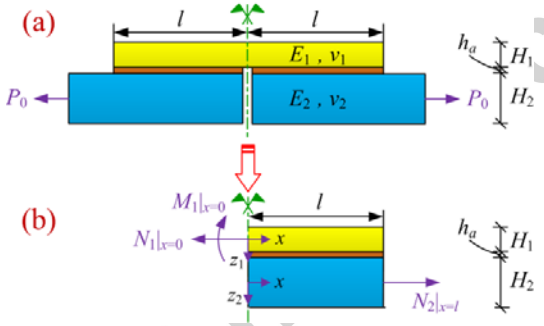

Fig. 3. (a) A single-strap joint under axial tensile loading; (b) reduced right-hand half portion of the joint.

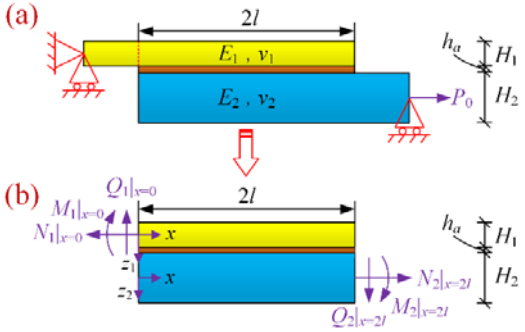

Fig. 4. (a) A single-lap joint under axial tensile loading; (b) schematic overlap region with boundary forces.

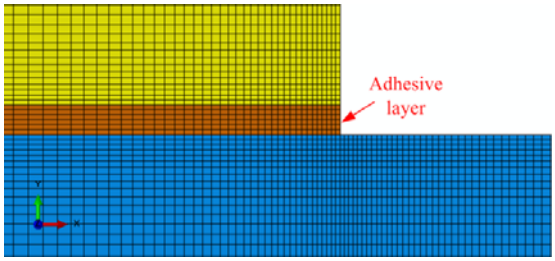

Fig. 5. Detailed 2D finite element mesh

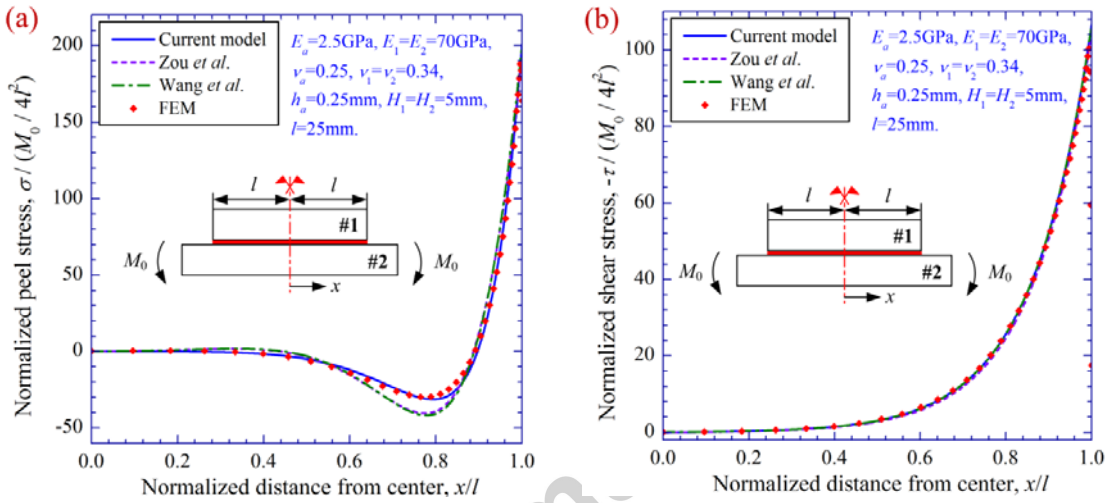

Fig. 6. Normalized adhesive stresses for a balanced stiffened plate/joint under bending: (a) peel stresses; (b) shear stresses.

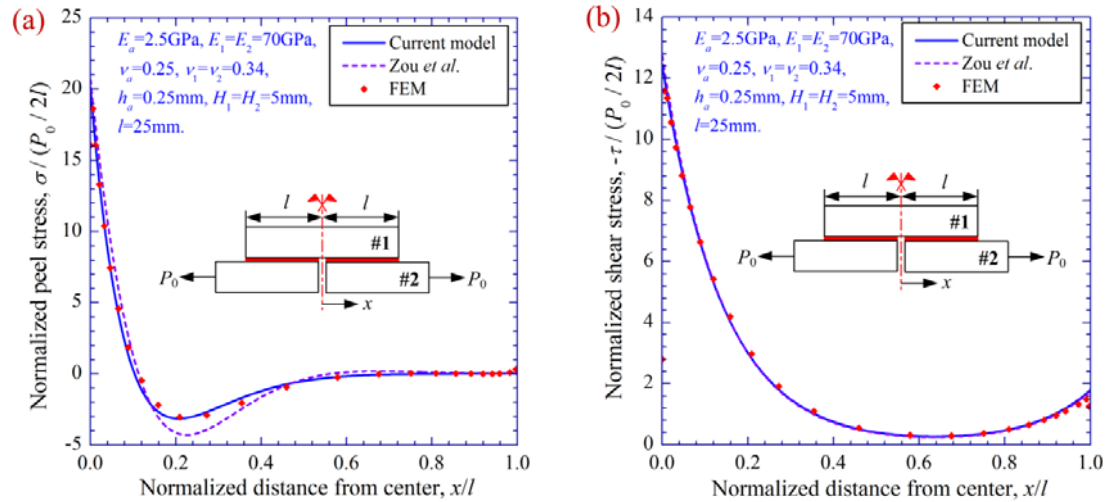

Fig. 7. Normalized adhesive stresses for a balanced single-strap joint under tension: (a) peel stresses; (b) shear stresses.

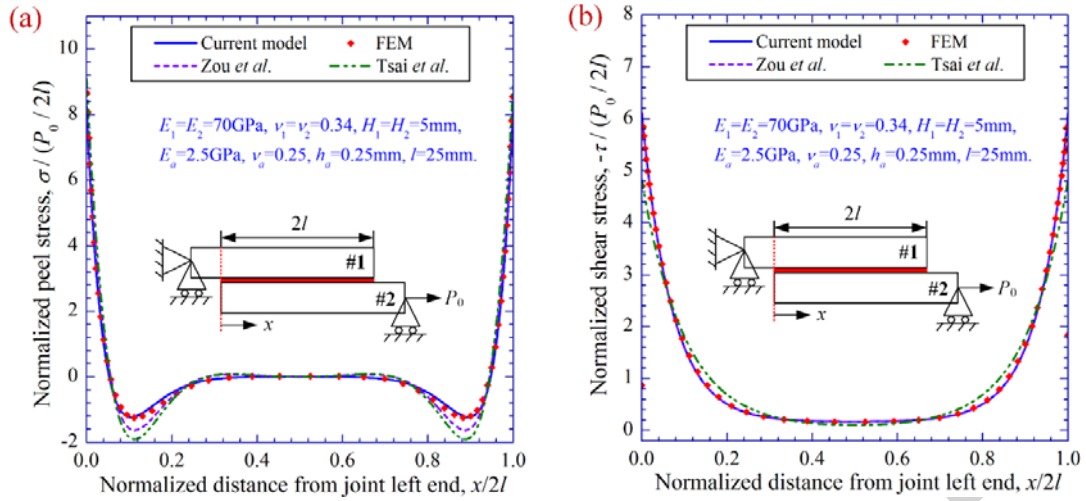

Fig. 8. Normalized adhesive stresses for a balanced single-lap joint under tension: (a) peel stresses; (b) shear stresses.

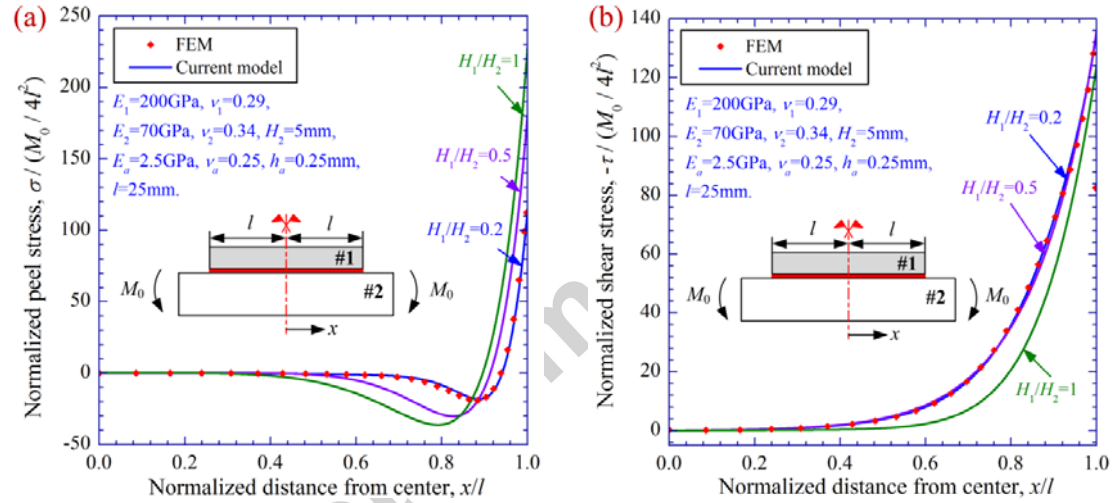

Fig. 9. Normalized adhesive stresses for an unbalanced stiffened plate/joint under bending: (a) peel stresses; (b) shear stresses.

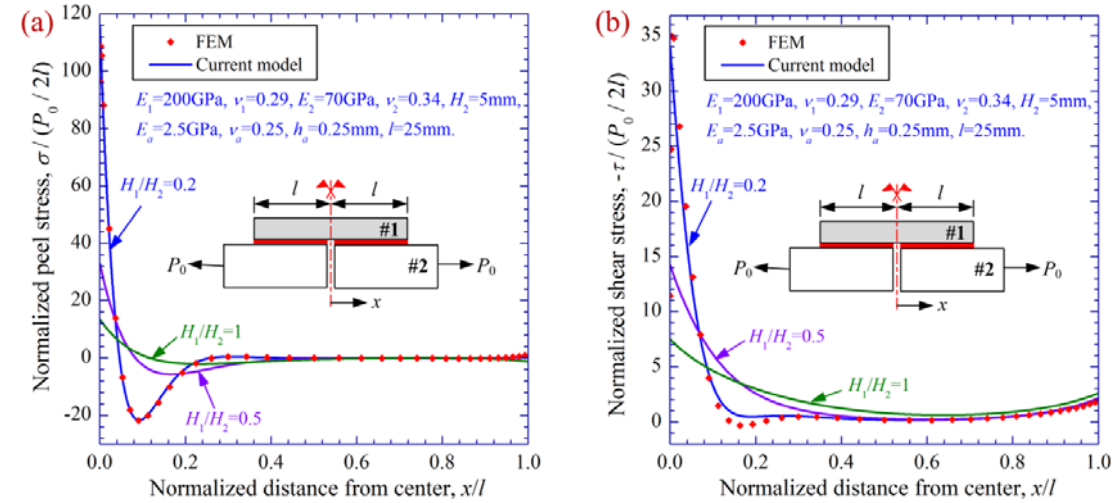

Fig. 10. Normalized adhesive stresses for an unbalanced single-strap joint under tension: (a) peel stresses; (b) shear stresses.

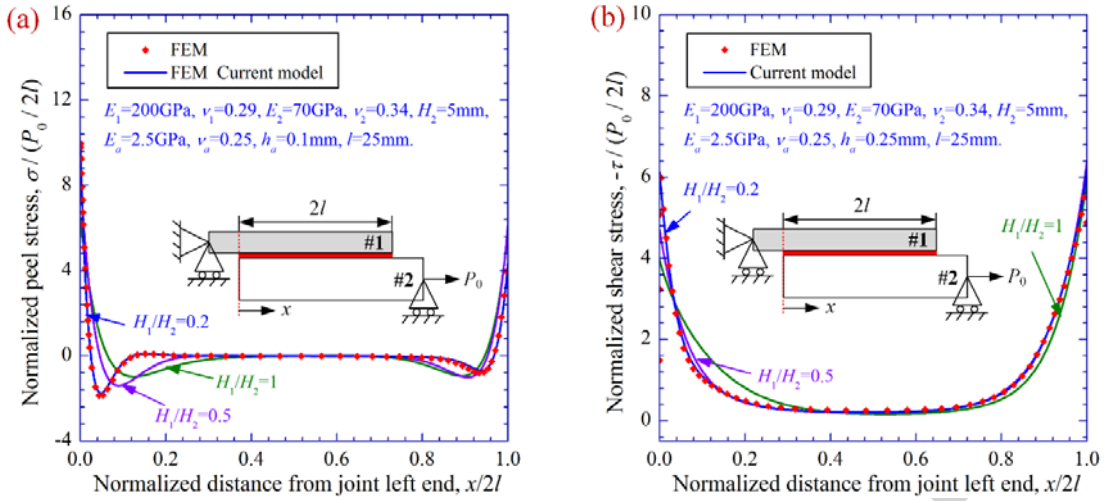

Fig. 11. Normalized adhesive stresses for an unbalanced single-lap joint under tension: (a) peel stresses; (b) shear stresses.

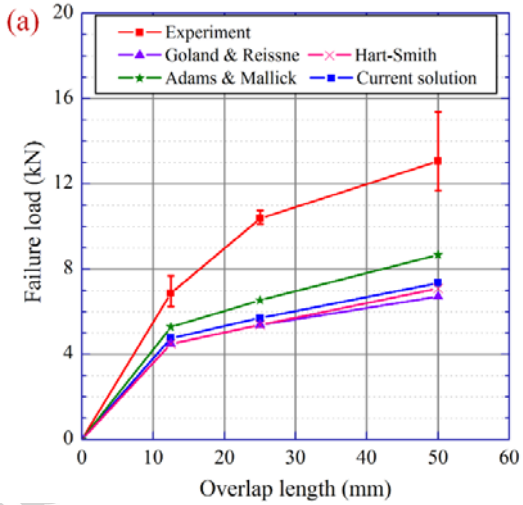

Fig. 12. Verification of the prediction of failure load considering the brittle adhesive (Redux 326) for 12.5, 25 and 50 mm overlap lengths. The experimental data are from Refs. 21 and 25.